The L561A Substitution in the Nascent Base-Pair Binding Pocket of RB69 DNA Polymerase Reduces Base Discrimination[†]

Hong Zhang,[‡] Chanu Rhee,[‡] Anna Bebenek,[§] John W. Drake,[||] Jimin Wang,[‡] and William Konigsberg*[,‡]

Department of Molecular Biophysics and Biochemistry, Yale University, 333 Cedar Street, New Haven, Connecticut 06520, Institute of Biochemistry and Biophysics, Polish Academy of Science, Pawinskiego 5A, 02-106 Warsaw, Poland, and Laboratory of Molecular Genetics, National Institute of Environmental Health Sciences, 111 South Alexander Drive, Research Triangle Park, North Carolina 27709-2233

ABSTRACT: Several variants of RB69 DNA polymerase (RB69 pol) with single-site replacements in the nascent base-pair binding pocket are less discriminating with respect to noncomplementary dNMP incorporation than the wild-type enzyme. To quantify the loss in base selectivity, we determined the transient-state kinetic parameters for incorporation of correct and all combinations of incorrect dNMPs by the exonuclease-deficient form of one of these RB69 pol variants, L561A, using rapid chemical quench assays. The L561A variant did not significantly alter the k_{pol} and K_D values for incorporation of correct dNMPs, but it showed increased incorporation efficiency (k_{pol}/K_D) for mispaired bases relative to the wild-type enzyme. The incorporation efficiency for mispaired bases by the L561A variant ranged from $1.5 \times 10^{-5} \, \mu M^{-1} \, s^{-1}$ for dCMP opposite templating C to $2 \times 10^{-3} \, \mu M^{-1} \, s^{-1}$ for dAMP opposite templating C. These k_{pol}/K_D values are 3−60-fold greater than those observed with the wild-type enzyme. The effect of the L561A replacement on the mutation frequency *in vivo* was determined by infecting *Escherichia coli* harboring a plasmid encoding the L561A variant of RB69 pol with T4 phage bearing a mutant *rII* locus, and the rates of reversions to *rII*+ were scored. The exonuclease-proficient RB69 pol L561A displayed a weak mutator phenotype. In contrast, no progeny phage were produced after infection of *E. coli*, expressing an exonuclease-deficient RB69 pol L561A, with either mutant or wild-type T4 phage. This dominant-lethal phenotype was attributed to error catastrophe caused by the high rate of mutation expected from combining the pol L561A and exo− mutator activities.

DNA polymerase is the central component of replicases that are responsible for faithfully copying DNA. Although all four dNTPs[1] are potential substrates, replicative DNA polymerases are able to limit the incorporation of mismatched bases to about one in a million (for reviews see refs *1−8*). Although this error frequency is acceptable for phage replication, it is still far too high to maintain genetic integrity during cell proliferation in more complex organisms. To increase fidelity, cells have a number of mechanisms for correcting errors, including the ability of the replicative DNA polymerase itself, or an associated subunit, to excise misincorporated bases. In addition, there are specialized DNA polymerases that confront DNA damage inflicted by radiation, oxidation, alkylating agents, and so forth, which block the progress of replicative polymerases (*6, 9−20*). These

DNA polymerases, as exemplified by members of the Y family, are less selective toward incoming dNTPs and have lower catalytic efficiencies for correct insertion compared with replicative polymerases (*21, 22*). On the other hand, misincorporation results in reduced primer extension rates, providing an opportunity for the exonuclease activity of the replicative polymerases, or their associated subunits, to remove mismatched bases at the 3′-terminus of the primer before they become part of the DNA duplex (*23, 24*). Because the rate of extension beyond a mismatch is also slower than continued DNA synthesis from a correctly base-paired primer−template terminus, the opportunity for error correction by the exo activity of the polymerase or replicase is further increased (*24*).

In the continuing quest to understand the molecular basis for base discrimination exhibited by replicative DNA polymerases, we have chosen to study the DNA polymerase from bacteriophage RB69. RB69 pol, like its closely related homologue T4 DNA polymerase, belongs to the B family and has sequence similarities with many eukaryotic DNA pols such as human pol α (*25*). The crystal structures of the Apo form of the RB69 pol and several RB69 pol−DNA complexes have been solved (*12, 26−29*). The palm, fingers, and thumb domains, which are clearly recognizable in RB69 pol, are common features shared by many DNA polymerases. The catalytic center for the phosphoryl transfer reaction lies in the palm, the most highly conserved domain among all

* To whom correspondence should be addressed. Phone, (203) 785-4599; fax, (203) 785-7979; e-mail, William.Konigsberg@yale.edu.
‡ Yale University.
§ Polish Academy of Science.
|| National Institute of Environmental Health Sciences.

[1] Abbreviations: RB69 pol, RB69 DNA polymerase; P/T, primer/template; ddP/T, dideoxy-terminated primer/template; Ni−NTA, nickel−nitrilotriacetic acid; dNTP, deoxy-nucleoside triphosphate; KF, Klenow Fragment.
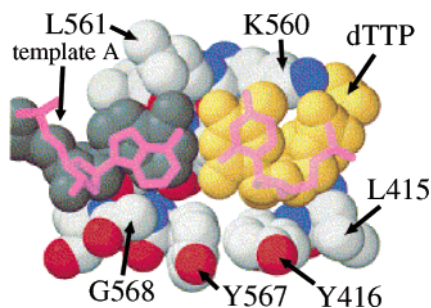
FIGURE 1: Space-filling model of residues in the fingers and palm domains that are part of the nascent base-pair binding pocket (*29*). Included are space-filling models of dTTP (gold) pairing with a templating A (gray). The structure of an A-form A−C mismatch (magenta sticks) was taken from PDB code 4O2D (*46*). The view is along the axis of the P/T−DNA, which is omitted for clarity.

the polymerases (*30*). Amino acid residues that comprise the nascent base-pair binding pocket of RB69 pol in the "closed" conformation have been identified and are shown in Figure 1 (*29*). The interactions and putative function of the side chains of these residues with the incoming dNTPs are as follows: (i) Y416 functions as a "sugar gate" to distinguish between the ribose and the deoxyribose moieties associated with the incoming nucleoside triphosphate (*31*); (ii) K560 interacts with the nonbridging α and γ oxygens in the triphosphate moiety of the incoming dNTP (*32*); and (iii) the hydroxyl group of residue Y567 forms a hydrogen bond with the minor groove edge of the DNA duplex at the primer−template terminus (*29*). Replacement of the aromatic side chain of Y567 with a methyl group (Y567A) reduces base discrimination against mismatched bases without affecting the rate of incorporation for complementary dNMPs (*33, 34*). As part of this nascent base-pair binding pocket, L415, Y416, and Y567 are involved in hydrophobic interactions with the minor groove of the nascent base pair. The rear wall of this binding pocket, which includes residues L561, N564, and S565 as shown in Figure 3 of ref *12*, is presumed to reinforce the coplanar arrangement of the nascent base pair (*12*). In accordance with the ternary structure of RB69 pol (*29*), the side chain of L561 is an obvious protrusion into the nucleotide binding pocket that may clash with a bulge on the major groove side of a mispair. Even though this steric clash is estimated to cause only about 0.1−0.2 Å of overlap, it may be sufficient to account for the selectivity against purine−purine mismatches, since these mispairs need more space than is available in the binding pocket. The amino acid residues cited above define a very tight binding pocket that has evolved to accommodate Watson−Crick base pairs but leaves little space for water molecules or for bulges caused by incorrect geometry of noncomplementary base pairs.

We have previously reported that the RB69 pol Y567A variant exhibits reduced base selectivity and enhanced mutagenicity compared to the wild-type RB69 pol (*33, 34*). Here, we present *in vivo* and *in vitro* data on the consequences of replacing L561 with Ala. We also discuss the frequency and types of errors that the RB69 pol L561A variant generates in vivo. In addition, the kinetic parameters for the wild-type enzyme and the L561A variant have been determined in vitro under single-turnover conditions with matched and all combinations of mismatched incoming dNTPs. We compared our results with those found for the

Klenow fragment (KF), where similar types of studies have been carried out (*35, 36*). We have also placed various noncomplementary base pairs into the RB69 pol ternary complex in silico to see if the kinetic data from the wild-type and the L561A variant polymerase, with the mispaired bases, could be rationalized by modeling.

EXPERIMENTAL PROCEDURES

Materials. [γ-^{32}P]ATP was obtained from Perkin-Elmer Life Sciences, Inc.; dNTPs were obtained from New England Biolabs. Electrophoresis reagents were from American Bioanalytical Corp. Oligonucleotides were synthesized by the W. M. Keck Foundation Biotechnology Resource Laboratory at the Yale University Medical School. All other chemicals were analytical grade. The "parental" RB69 pol and the L561A variant used for the kinetic studies carry the D222A/D327A double replacement that eliminates the 3′-5′ exonuclease activity of the polymerase.

Construction, Expression, and Purification of the L561A Variant of RB69 Pol. Site-directed mutagenesis to create the L561A variant was carried out using the Stratagene Quikchange PCR protocol. The cDNA encoding the RB69 pol L561A variant was sequenced to confirm the identity of the altered codon and to ensure that no other changes were inadvertently introduced during PCR amplification. This cDNA was then cloned into the SP72 vector (Promega) for the *in vivo* studies and into the pET21b plasmid (Novagen) for the *in vitro* studies. Expression and purification of the RB69 pol L561A variant was carried out as previously described (*32*), with the exception that a Ni−NTA affinity column was used for the initial purification since there were six His residues appended at the C-terminus when it was expressed from the cDNA cloned into the pET 21b vector. The 200 mM imidazole eluate from the Ni−NTA column was pooled after checking for the identity and purity of the fractions by SDS−PAGE. After removal of most of the imidazole by dialysis, the polymerase was loaded onto a Source 30Q column and eluted with a linear gradient of increasing KCl concentration. The eluted fractions were checked for purity by SDS−PAGE. Fractions containing >98% purity of the RB69 pol L561A variant were pooled, and the concentration was determined by the Bradford assay. The pooled fractions were then dialyzed against standard polymerase storage buffer (*26*) and frozen in small aliquots at −80°C for future use.

Single-Turnover Experiments. Rapid chemical quench experiments were carried out using the KinTek Quench Flow Instrument (Model RQF-3, KinTek Corp., University Park, PA). For slower reactions requiring sampling at time intervals longer than 20 s, aliquots were taken manually, quenched with 0.2 M EDTA, and subjected to electrophoresis in 20% acrylamide gels with 8 M urea as previously described (*37*). Single-turnover experiments were performed as previously described (*32*). The concentration of the incoming dNTPs were varied to determine K_D and k_{pol} values. The primer−template sequences used in this work are given in Table 1.

Data Analysis. Data from single-turnover experiments fit best to the equation for a single exponential. The apparent dissociation constant, K_D, for dNTP binding to the RB69 pol−P/T complex, was calculated by fitting data from the k_{obs} versus dNTP concentration (see Figure 2B as an

Table 1: Sequences of Primer−Templates Used for Kinetic Studies

Primer/template	Sequences*		dNTP used for assays
13/20CA	5′ −CCGACCACGGAAC		dATP, dCTP
	3′ −GGCTGGTGCCTTG**C**AAAAAA		
13/20CG	5′ −CCGACCACGGAAC		dGTP, dTTP
	3′ −GGCTGGTGCCTTG**C**GGTTTT		
13/20GA	5′ −CCGACCACGGAAC		dATP, dGTP
	3′ −GGCTGGTGCCTTG**G**AAAAAA		
13/20GC	5′ −CCGACCACGGAAC		dCTP, dTTP
	3′ −GGCTGGTGCCTTG**G**CCCCCC		
13/20AC	5′ −CCGACCACGGAAC		dATP, dCTP
	3′ −GGCTGGTGCCTTG**A**CCCCCC		
13/20AG	5′ −CCGACCACGGAAC		dGTP, dTTP
	3′ −GGCTGGTGCCTTG**A**GGTTTT		
13/20TC	5′ −CCGACCACGGAAC		dATP, dCTP
	3′ −GGCTGGTGCCTTG**T**CCCCCC		
13/20TG	5′ −CCGACCACGGAAC		dGTP, dTTP
	3′ −GGCTGGTGCCTTG**T**GGTTTT		
	* The templating bases are in boldface.		

Table 2: Mutator Activities of RB69 Pol[l561a] Exo[+] in Reversion Tests[a]

rII tester mutation	mutations scored	reversion rate $\mu \times 10^8$			
		Pol[+]	Pol[L561A]	Pol[L561A]/Pol[+]	*P*
131	+1	9.0	11	1.2	0.041
UV232	−1	1.0	4.4	4.5	0.0003
UV256	G·C → A·T	6.4	17	2.6	0.0002
UV375	A·T → any	1.6	6.6	4.3	0.0002

[a] The *P* values were determined from two-tailed Mann−Whitney tests. Adding the numbers in the fifth column and dividing them by 4 gives the average mutator factor of 3.2.

example) to the hyperbolic equation; $k_{obs} = (k_{pol}[S]/(K_D + [S])$, where k_{pol} is the maximum rate of dNMP incorporation.

Mutation Tests in Vivo. Reversion tests using T4 *rII* reporter mutations were performed as described (*33*). In these tests, a T4 strain carrying an *rII* mutation and a double-amber mutation in the DNA pol gene (gene *43*) was used to infect an *Escherichia coli* strain carrying a plasmid that expresses an RB69 gene *43* which may be either wild-type or mutant. This system exhibits strong complementation and approximately normal mutation rates. The resulting T4 progeny can be screened for four types of *rII*[+] revertants (*38*): *rII131* reverts mainly by +1 (A$_5$ → A$_6$); *rIIUV232* by −1 (A$_3$ → A$_2$); *rIIUV256* by base-pair substitutions at a G·C mainly by transitions; and *rIIUV375* by both transitions and transversions at three adjacent A·T sites. Reversion rates (μ) were calculated as $\mu = f/\ln(N\mu)$ where *f* is the revertant frequency and *N* is the final population size. Posted reversion rates are medians of 17 stocks for pol[+] and of 14 stocks for RB69 pol L561A.

DNA Synthesis in Vivo. The measurements were performed as described (*33*), except that the cells were grown in LB medium instead of M9SB medium to achieve vigorous growth. [³H]Thymidine at 5 μCi/mL and specific activity 2 mCi/mmol was used. The endogenous content of thymine and/or thymidine in LB medium was low and was negligible in these experiments.

Modeling. Modeling of mismatches into the ternary RB69 pol complex (*29*) has been carried out using two approaches: (i) superimposition of the four atoms that define the two glycosidic bonds of the base pairs and (ii) superimposition of the four atoms that define the glycosidic bond of the dNTP and the two atoms immediately next to N1 or N9 of the glycosidic bond that defines its base plane. In the second approach, the sugar and triphosphate group of the incoming dNTP are fixed so that their positions are identical to dTTP observed in the ternary structure of RB69 pol (*29*). However, in several instances, the opposing nucleotide residue deviated by more than 15° from the base plane (see Discussion), causing it to sterically clash with residues in the nucleotide binding pocket of the polymerase. We will address both types of modeling in an attempt to elucidate the structural basis for fidelity.

RESULTS

The primary aim of this study was to evaluate the contribution of L561, a conserved residue in the nucleotide binding pocket of RB69 pol, to base selection. We also wanted to determine the effect of changing L561 to Ala on the generation of mutations in T4 phage DNA synthesized *in vivo*. To initiate this work, we replaced L561 with Ala in an exonuclease-deficient derivative of RB69 DNA pol and determined k$_{pol}$ and K_D values for the L561A variant with correctly matched and all combinations of mismatched bases under single-turnover conditions. To obtain data on mutator activities, we tested the plasmid-borne L561A constructs in vivo after infecting the plasmid-bearing *E. coli* cells with T4 phage and estimated the reversion rates of T4 *rII* mutations. These experiments were done with both the exo[+] and exo[−] forms of the L561A variant to assess the relative contributions of the L561A replacement alone, and in combination with mutations that eliminate the exo activity, to the observed mutation frequency.

Characterization of L561A Constructs in Vivo. The results of reversion tests using T4 *rII* mutations are described in Table 2. RB69 pol[L561A] exo[+] is, at most, a very weak mutator for single-base additions in the *rII131* test and is a weak mutator for single-base deletions in the *rIIUV232* test. The enzyme variant is also a weak mutator in two tests for base-pair substitutions. An important constraint applies to these results: the mutabilities of particular sites may vary by several orders of magnitude and also depend on the DNA polymerase.

In contrast to RB69 pol[L561A] exo[+], none of several RB69 pol[L561A] exo[−] constructs supported the growth of T4 phage whose own DNA polymerase gene (gene *43*) was disabled by a pair of early amber mutations (Table 3). In addition, even wild-type T4 phage replicated poorly when the host cells expressed RB69 pol[L561A] exo[−]. Similar results were obtained with parallel constructs in which the RB69 exo activity was disabled by either a double D222A/D327A or a single D222A substitution. When the single D222A substitution in the exo domain was reconverted to D222, T4 phage could again grow in cells expressing RB69 pol[L561A] exo[+] (data not shown).

Previously, two mechanisms have been described for such dominant lethality. In one, the RB69 pol variant is catalytically insufficient but is produced in quantities sufficient to translationally suppress the T4 pol from the infecting T4 phage (*33, 39, 40*). In the other, the RB69 pol variant produces a mutator effect so great that almost no progeny remains free of lethal mutations (error catastrophe or mutational meltdown) (*33*). Little DNA synthesis occurs with

Table 3: T4 Growth and DNA Synthesis Supported by RB69 Pol Constructs[a]

RB69 pol	T4 *43amam* growth	T4 *43+* growth	relative DNA synthesis
pol+ exo+	+	+	1.0
pol+ exo−	+	+	0.9
pol^{L561A} exo+	+	+	0.8
pol^{L561A} exo−	−	±	0.4
pol^{L561A} exo^{D222A}	−	±	0.5
pol^{Y567F} exo+	−	+	0.06

[a] Exo− carries both of the exo-inactivating D222A and D327A mutations. Phage growth was estimated by spot tests as described (*40*). Relative DNA synthesis was normalized to [³H]thymidine incorporation between 22 and 37 min after infection with T4 *43am*. The value of 1.0 for RB69 pol+ exo+ represents 3.2×10^5 dpm ³H per 10^7 infected cells.

suppressed translation of gp43 mRNA, whereas abundant DNA synthesis can occur in the presence of hypermutation. We therefore measured DNA synthesis in infected cells at a time when host DNA synthesis had ceased completely (Table 3). As reported previously (*33*), the double D222A/D327A exo-domain replacement in the pol+ exo− construct had only a small impact on DNA synthesis. The single pol-domain replacement, L561A, also barely affected the level of DNA synthesis. Constructs with replacements in both the pol and exo domains had a moderate impact on DNA synthesis, reducing it by about half (Table 3). This effect is similar to that observed with the RB69 pol^{Y567A} exo− construct, in which relative DNA synthesis was reduced to 0.6 (*33*). Independent evidence implicated lethal hypermutation in the inability of the pol^{Y567A} exo− construct to support T4 phage replication: the mutation rate in the double-mutator mutant was increased roughly 2400-fold, implying a genomic rate of about seven mutations per chromosome replication (*33*). In contrast, the catalytically defective pol^{Y567F} exo− construct, which is also unable to support T4 phage replication, was able to support only 0.06% of normal DNA replication, a value similar to the 0.04% reported previously (*33*). We therefore suspect that the inability of the Pol^{L561A} exo− construct to support phage growth reflects lethal hypermutation. Although the average mutator factor of the pol^{L561A} exo+ construct in reversion tests is only about 3-fold (Table 2 footnote), the combination of this factor with the very strong exo− mutator factor, about 500-fold (*33*), may be enough to produce lethal hypermutation.

Kinetic Parameters for Incorporation of Correct dNMPs under Single-Turnover Conditions by the Parental Enzyme and by the L561A Variant. The use of synthetic oligonucleotides with defined sequences, shown in Table 1, made it possible to study the insertion kinetics of a single nucleotide (either correct or incorrect) opposite a given templating base. Before testing the capability of the RB69 pol L561A variant to incorporate mispaired dNMPs, we first determined the k_{pol} and K_D values for the complementary base pairs, for instance dT−A and dG−C pairs (where dT and dG are the incoming dNTPs and A and C are the templating bases, respectively). These values were then compared to those obtained for the same nascent base pairs by using the parental enzyme, as shown in Table 4. The K_D values were in the same range (17−70 μM) for both the parental RB69 pol and the L561A variant. On the other hand, the k_{pol} values for the L561A

variant were reduced by roughly 50% relative to that of the parental enzyme. The relative efficiencies shown in the last column of Table 4 are close to 1, except for the dT−A pair which is 0.4. This strongly suggests that the L561A variant is only slightly less efficient than the parental enzyme for correct nucleotide incorporation.

Kinetic Parameters for Incorporation of Mispaired dNMPs by the Parental Enzyme and by the L561A Variant. Having evaluated the transient-state kinetic parameters for the correct base-pair combinations, we then estimated K_D and k_{pol} values for the 12 different combinations of mispaired bases. A summary of the data is shown in Table 4. The general picture that emerges is that the L561A variant incorporates mispaired bases with much greater efficiency than the parental enzyme with k_{pol}/K_D ratios for the L561A variant versus the parental enzyme ranging from ∼3- to 60-fold. An example of how the kinetic parameters were determined for a mismatch is shown in Figure 2, where dGTP is the incoming nucleoside triphosphate and A is the templating base. Increasing concentrations of dGTP were used, and the rates of product formation were plotted as a function of time (Figure 2A). The observed rate constants (k_{obs}) were then plotted versus dGTP concentration to obtain the K_D and k_{pol} values (Figure 2B). We note that when the K_D values are greater than 2 mM, as observed with dC−A, dC−C, and dC−T mispairs, they represent the best approximation from extrapolation of k_{obs} versus dNTP concentration. Whenever the maximum rate of product formation was not reached at the highest dNTP concentration, the apparent K_D could only be roughly estimated. At dNTP concentrations exceeding 5 mM, there was also an apparent inhibition of the pol reaction. In these cases, the reported k_{pol} values are only approximate, their precision depending on the affinity of the incoming dNTP for the enzyme−P/T complex.

It is clear from the data in Table 4 that the parental enzyme has dramatically decreased incorporation efficiency for mismatched incoming nucleotides. The dC−C pair has the lowest value ($3.6 \times 10^{-7} \mu$M^{-1} s^{-1}). The overall selectivity of the parental enzyme comes from the strong discrimination against all mispaired bases as demonstrated by the striking difference in k_{pol}/K_D values, with 2−7 μM^{-1} s^{-1} for complementary base pairs and $10^{-4}−10^{-7} \mu$M^{-1} s^{-1} for mismatched base pairs. By contrast, the L561A variant appears to have reduced selectivity for all mispairs compared to the parental enzyme. The highest K_D values for the L561A variant during misincorporation were observed when dCTP was the incoming nucleotide. For instance, in the case of dC−C, the K_D was about 2 mM, and for dC−T, the K_D was about 1.5 mM. On the other hand, the dT−G mispair had the lowest K_D (28 μM), similar to the value for complementary base pairs. With respect to k_{pol} values, the dA−C and the dT−C mispairs had the highest values (0.8 s^{-1}), whereas the dG−A mispair had the lowest value (0.01 s^{-1}). The dC−T and dG−T mispairs happened to have similar k_{pol} values, but the K_D for dG−T was significantly lower than that for dC−T, which accounts for the difference in efficiencies between these two sets of mispaired bases. Moreover, the L561A variant has different k_{pol} and K_D values when the incoming and the templating bases are switched (i.e., dC−A versus dA−C). Compared to the parental enzyme, the increase in misincorporation efficiencies by the L561A variant for these two mispairs are 46-fold for the dA−C pair

Table 4: Transient Kinetic Parameters for dNMP Incorporation by the Parental RB69 Pol and the L561A Variant[a]

dNTP vs N	K_D			k_{pol}			k_{pol}/K_D		
	WT	L561A	w/v	WT	L561A	v/w	WT	L561A	v/w
dA−T	*50*	*30*	*1.67*	*220*	*108*	*0.49*	*4.4*	*3.6*	*0.8*
dC−G	*69*	*50*	*1.38*	*200*	*101*	*0.5*	*2.9*	*2.0*	*0.7*
dG−C	*26*	*17*	*1.53*	*167*	*89*	*0.53*	*6.4*	*5.1*	*0.8*
dT−A	*42*	*51*	*0.82*	*240*	*115*	*0.48*	*5.7*	*2.3*	*0.4*
dA−A	811	155	5.23	0.013	0.03	2.3	1.6×10^{-5}	2.5×10^{-4}	15.6
dA−C	1800	368	4.89	**0.08**	0.75	**9.4**	4.4×10^{-5}	2.0×10^{-3}	**45.5**
dA−G	909	310	2.93	0.004	0.03	7.5	4.3×10^{-6}	8.4×10^{-5}	19.5
dC−A	**4500**	537	8.38	**0.77**	0.26	**0.3**	1.7×10^{-4}	4.8×10^{-4}	**2.8**
dC−C	3363	2010	1.67	0.001	0.03	30	3.6×10^{-7}	1.5×10^{-5}	41.6
dC−T	2085	1467	1.42	0.013	0.14	11	6.2×10^{-6}	9.5×10^{-5}	15.3
dG−A	784	228	3.44	0.003	0.01	3	4.1×10^{-6}	4.8×10^{-5}	11.7
dG−G	761	161	4.73	0.011	0.11	10	1.5×10^{-5}	6.8×10^{-4}	45.3
dG−T	725	251	2.89	0.041	0.18	4.4	5.7×10^{-5}	7.2×10^{-4}	12.6
dT−C	1715	507	3.38	0.09	0.8	8.9	5.3×10^{-5}	1.6×10^{-3}	29.8
dT−G	1986	**28**	70.93	0.14	0.05	0.36	7.0×10^{-5}	1.8×10^{-3}	25.7
dT−T	1391	205	6.79	0.015	0.13	8.7	1.1×10^{-5}	6.3×10^{-4}	57.6

[a] In the first column, dA, dC, dG, and dT are incoming dNTPs. A, C, G, and T are templating bases denoted in the table heading as N. K_D values are in μM, k_{pol} values are in s^{-1}, and k_{pol}/K_D ratios are expressed as $\mu M^{-1} s^{-1}$. The last column on the right is the catalytic efficiency ratios $(k_{pol}/K_D)_v/(k_{pol}/K_D)_w$ between the L561A variant (v) and the wild-type (w). It can also be calculated by the product of two ratios: $K_D(w/v)$ (fourth column) and $k_{pol}(v/w)$ (seventh column). Italics and bold face within the table are discussed and emphasized in the text. Standard deviation (SD) for the K_D values were $\pm15\%$ for K_D values below 100 and varied from ±20 to $\pm30\%$ for K_D values between 100 and 1500. For K_D values above 1500, the SD was $\pm40\%$. SD for k_{pol} values were $\pm15\%$.
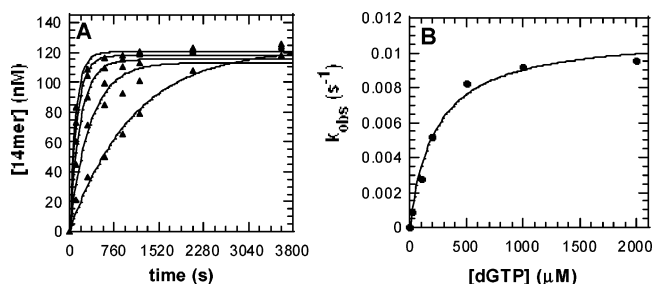

FIGURE 2: Determination of K_D and k_{pol} values for the incorporation of the dG−A mispair by the L561A variant under single-turnover conditions. (A) For a given dGTP concentration, L561A variant (2 μM) and 13/20mer (400 nM) were preincubated and then mixed rapidly with an equal volume of dGTP in Tris-HCl buffer, pH 7.5, containing 20 mM MgCl$_2$ to start the reaction. The reaction was quenched at several time points and was analyzed by gel electrophoresis. The dGTP concentrations (from the bottom to the top) were 20, 100, 200, 500, and 1000 μM, respectively. The solid lines represent the best fit of the data to a single exponential. (B) The dGTP concentration dependence of k_{obs} fit a rectangular hyperbola and was used for K_D and k_{pol} determination as described in Experimental Procedures.

and 3-fold for the dC−A pair (last column of Table 4). Replacement of the side chain of L561 with a methyl group affects base selection differently depending on the position and identities of the base pairs.

DISCUSSION

Mutations Produced in Vivo by RB69 Pol L561A. In previous studies, we reported the consequences of replacing Y567, a residue forming part of the nucleotide binding pocket, with Ala and Phe (*34*). When we extended this study to the L561A variant, we found that, in the exo$^+$ background, the RB69 pol L561A derivative was a weak mutator in all the tests described in Results. As noted above, the mutabilities of different sites in the target DNA may vary by several orders of magnitude, and the variation is dependent on the polymerase. Thus, mutator factors determined by reversion tests in vivo are unlikely to correspond precisely to what

would be predicted from kinetic parameters determined *in vitro*. An alternative explanation of the smaller mutator factors seen with the exo$^+$ form of the L561A variant *in vivo* than with the exo$^-$ L561A variant *in vitro* might be that the L561A replacement enhances partitioning of the DNA from the pol to the exo site, adding an antimutator component to the insertion−mutator component of fidelity.

When the L561A was in the exo$^-$ background, it exhibited dominant lethality, a result consistent with what we had observed previously with the Y567A variant in the exo$^-$ background which we attributed to error catastrophe (*33*). We suggest that "error catastrophe" is also responsible for the dominant-lethal effect found with the L561A variant.

The Kinetic Behavior of the RB69 Pol L561A Variant. The efficiency of the L561A variant relative to wild-type (WT) for incorporating correct dNMPs varied between 0.4 and 0.8. These values resulted from the slightly higher binding affinity and the 50% lower k_{pol} values exhibited by the L561A variant compared to WT for complementary dNTPs (Table 4). These unexpected results are similar to what we reported for the Y567A variant (exo$^-$) of RB69 DNA pol (*34*). However, it differs from what has been observed for other DNA polymerase variants. For example, a KF variant bearing a single mutation in the active site had a significantly lower k_{pol} and a much higher K_D for complementary dNTPs than wild-type KF (*35*, *36*). There are a number of mechanisms that might account for how discrimination against incorrect dNTPs could be achieved during evolution. Beard et al. (*41*) have observed a high degree of correlation between fidelity and catalytic efficiency for correct dNTPs for all naturally existing DNA polymerases—the higher the efficiency, the higher the fidelity. However, the catalytic efficiency for incorporation of incorrect dNMPs or, more precisely, the catalytic *inefficiency*, plays only a small role in contributing to fidelity across the landscape of different classes of DNA polymerases. Through evolution, DNA polymerases may have already achieved the lowest possible catalytic *inefficiency* for incorrect dNTPs, while continually improving

catalytic efficiency for correct dNTPs. In accordance with this hypothesis, one might expect that each active site residue contributes to improving the catalytic efficiency for correct dNTPs, and any point mutation would decrease it. This appears to be the case for KF (*35*, *36*) and for many other DNA polymerases. However, our data on the L561A variant presented here, as well as our earlier results on Y567A, do not support this idea, since the replacement of the side chains of Y567 and L561 with methyl groups fail to reduce the catalytic efficiency for insertion of the correct dNTPs.

Our data on RB69 pol L561A show that one of the functional roles of L561 is to suppress misinsertion by lowering the catalytic efficiency for mispairs. This suggests that the side chain of L561 may interact with the incoming nucleotides. Among all 12 mispairs tested, the effect of the L561A replacement on transient-state kinetic parameters is also reflected by decreases in K_D of up to 71-fold and increases in k_{pol} of up to 30-fold relative to the parental enzyme. An exception to the high K_D values observed for the mispairs with the L561A variant is the dT−G mispair, which has a K_D similar to the correct dC−G pair, implying that the geometry of the dT−G mispair does not interfere with ground-state binding but does perturb the alignment of the α-phosphorus atom of the incoming dTTP and the 3′-OH of the primer terminus resulting in a greatly reduced k_{pol} (Table 4). Moreover, mispairs involving the same bases exhibit quite different kinetic parameters when the positions, either as the incoming dNTP or the templating base, are reversed. The catalytic efficiency exhibited by the L561A variant increased 46-fold for the dA−C pair and 3-fold for the dC−A pair compared to the parental enzyme. This is due to the variation in k_{pol} values relative to those of the parental enzyme. This change, compared to the wild-type k_{pol}, differs by 31-fold between dA−C and dC−A pairs (Table 4, column 7). In fact, only the dC−A and the dT−G mismatches have further reduced k_{pol} ratios in comparison to the parental enzyme. The difference in k_{pol} ratios may imply somewhat different transition states which are beyond our capability of modeling. Similar position-dependent observations have been reported for the Klenow Fragment (*35*, *36*). Our results with the L561A variant are consistent with the accepted notion that active-site geometry is involved in base selection. To relate our kinetic results with the L561A variant to structural features of the enzyme−P/T complexes, one needs to examine structures of catalytically competent complexes with mispairs, either available from crystal structures or derived from computation and modeling. To date, no ternary complexes of any DNA polymerases with mispairs in the insertion site have been reported, probably because these incorrect nascent base pairs are metastable as the incorrect dNTPs have high K_D values for incorporation (Table 4, column 2). While our data on RB69 pol variants have identified several mismatched base pairs that could be used for capturing the desired complexes in crystal form, we have to rely on computational modeling of mismatched bases into the catalytically competent ternary complex of RB69 pol. These candidates include, for example, L561A using ddP/T having a templating G and an incoming dTTP, which would be expected to have a low K_D (Table 4). When the crystal structure of such a complex has been determined, one can extrapolate the results to the wild-type RB69 pol

Table 5: C1′−C1′ Distances for the Correct and Mismatched Base Pairs

base pair (primer−template)	distance (Å)	ref
A−T	10.3[a]	29
A−C	10.4[b]	47
G−G	11.2[c]	45
A−G	12.3[d]	44
T−C	8.7[e]	44

[a] This distance is 11.1 Å in the DNA duplex as reported by ref *42*. [b],[c] The distances of A−C and G−G mispairs were taken from crystal structures of DNA duplexes in the absence of protein. [d] This distance is 10.7 Å in the DNA duplex as reported by ref *48*. [e] This distance is 11.2 Å in the DNA duplex as reported by ref *49*.

and draw inferences about structural determinants of base selectivity.

Computer Modeling of Mismatches in the Ternary Complex of RB69 Pol. Mismatched bases have characteristic distances between the two C1′ atoms of paired nucleotides and angles between the two glycosidic bonds (*42*). While the C1′−C1′ distances of purine−pyrimidine mismatches are generally similar to the distances observed in Watson−Crick base pairs (Table 5), the ability of the polymerases to select correct base pairs against purine−pyrimidine mispairs relies partially on the depth of the minor groove, which is in contact with the side chain of Y567 (*34*, *43*). On the other hand, the C1′−C1′ distance for purine−purine mismatches is much greater than that for Watson−Crick base pairs (Table 5). The kinetic behavior of the polymerases is also affected by the width of the base pair in the nascent base-pair binding pocket. RB69 pol makes use of the Cα backbone of P361 and I362 for this purpose. These structural features cannot be easily altered by mutagenesis. In the case of pyrimidine−pyrimidine mismatches, the C1′−C1′ distance is much shorter than that of Watson−Crick base pairs (Table 5). Polymerases might not bind these base pairs tightly enough at the active site to allow for polymerization. Due to small size of this type of mismatch, the DNA polymerase may not desolvate the active site efficiently for catalysis to occur at a significant rate. If polymerases keep the templating base in the correct orientation for reaction, the incoming dNTP will be out of alignment for efficient phosphoryl transfer. The modeling of the three types of mispairs into the ternary complex of RB69 DNA polymerase requires high-resolution structures of mispairs in the E·P/T·dNTP complex. An attempt was made to determine the structures of all the possible mismatches in Bst pol I, an A family DNA polymerase (*44*). However, none of these structures represent a catalytically competent complex, which is what we need to rationalize our transient-state kinetic data. Among them, the G−T, T−G, T−T, C−T, A−G, and G−G mismatches were captured in the post-insertion state; the A−A, C−C, and G−A primer−template mismatches in the preinsertion state; and the T−C, A−C, and C−A mismatches were disordered (*44*). Nevertheless, the structures of these mispaired bases in duplex DNA provided the coordinates for modeling these mismatches into the ternary RB69 pol complex.

The Structural Basis for Discrimination of Purine−Pyrimidine Mismatches by the Parental Enzyme. The selection against the dC−A mismatch by the parental enzyme is due to its low binding affinity for the dC−A mispair in the ground state. In fact, this mismatch has the highest K_D
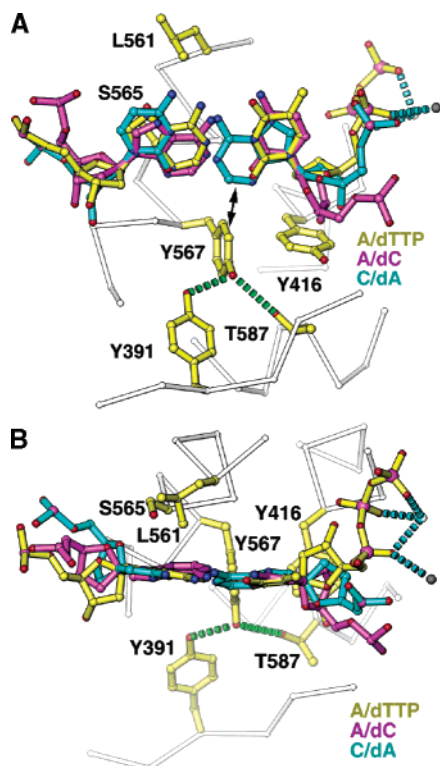
FIGURE 3: Structural basis for discrimination against purine−pyrimidine mismatches. Modeling of the dA−C (cyan) and dC−A (magenta) mismatches into the ternary RB69 pol structure (*29*) was carried out using four atoms defining two glycosidic bonds, because all purine−pyrimidine mismatches have nearly the same C1′−C1′ distance as the correct Watson−Crick base pairs. Note that, in all modeling figures, the primer strand and dNTP are on the right, and template strand and templating base are on the left. The incoming dNTPs are indicated with d (as in dA), whereas templating base are shown as C in the dA−C mismatch. Panels A and B are two orthogonal views of the model.

(4500 μM), which is more than 100-fold greater than that observed for Watson−Crick base pairs (Table 4). Modeling (Figure 3) shows that the dC−A mismatch would not fit the binding pocket very well, mainly because of a steric clash with the Y416 side chain, which could explain the observed high K_D value. For the dA−C mispair, the alignment of the α-phosphate and 3′-OH of the primer deviated from the optimal position, and as a result, the rate of catalysis was dramatically decreased. This implies a different transition state that is beyond the capability of our modeling. The L561A replacement created a slightly larger binding pocket, allowing mismatched base pairs to fit better. In fact, the K_D value of the L561A variant for the dC−A mispair decreased 8.4-fold compared to that of the parental enzyme. On the other hand, reorientation of the dA−C mispair led to a 5-fold decrease in K_D and a 9-fold increase in k_{pol} for the L561A variant, giving a 45-fold increase in misincorporation efficiency relative to the parental enzyme.

The Structural Basis for the Loss of Selectivity for Purine−Purine Mismatches by the L561A Variant. Residue L561 is located in a cluster of amino acids in the nascent base-pair binding pocket of RB69 pol (*29*) and forms part of the nonpolar region that restricts access of water to the reactants during phosphoryl transfer. It places steric constraints on the type of base pairs that can occupy the nucleotide binding pocket while still allowing the 3′-OH of the terminal primer and the α-phosphorus atom of the incoming dNTP to be
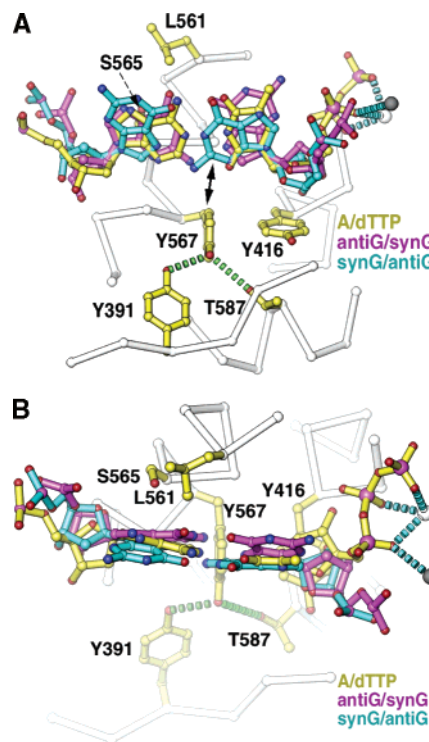

FIGURE 4: Modeling the dG−G mismatch into the ternary RB69 pol structure (*29*). The G−G mismatch was taken from ref *45* (PDB accession number 1D80) and imported into the ternary RB69 pol structure by superposition of four atoms of two glycosidic bonds with either primer G in syn conformation (magenta) or template G in syn conformation (cyan). Panels A and B are two orthogonal views of the model.

properly aligned for the transfer reaction. As we have demonstrated, the Ala for Leu substitution reduces discrimination against non-Watson−Crick base pairs, but the loss of selectivity varies considerably depending on the mispair. We are aware of the observed syn conformation of the primer 3′-terminal G in the G−G primer−template mismatch at the post-insertion site of Bst pol I (*44*); nevertheless, we previously modeled the anti conformation of the incoming dGTP at the insertion site of RB69 pol. We note that, at the post-insertion site, the base pair is not subject to the same geometric restrictions as the nascent base pair and the observed structure at the post-insertion site may not represent the conformational state that is relevant to the structure of the catalytically competent ternary complex.

When the nascent base pair, in the syn conformation with the G−G mismatch (*45*), is imported into the polymerase active site by superposition of the terminal G in the primer strand, the base clashes with one of the nonbridging oxygens in the triphosphate tail of the incoming dGTP. This requires that the templating nucleotide residue be in the syn conformation. When the templating G adopts the syn conformation, it has few stacking interactions with bases in the remaining duplex. Therefore, it might involve flipping the templating G from its favorable anti, to a syn conformation to allow the mispaired dGTP to be incorporated. This flipping may not occur frequently in solution in the absence of the polymerase. When the DNA is in a complex with the polymerase, flipping is restricted by the presence of bulky residues at the active site (*34*). We have argued that the incoming dGTP should be in the anti conformation when its ribosyl moiety is superimposed onto that of the ribosyl
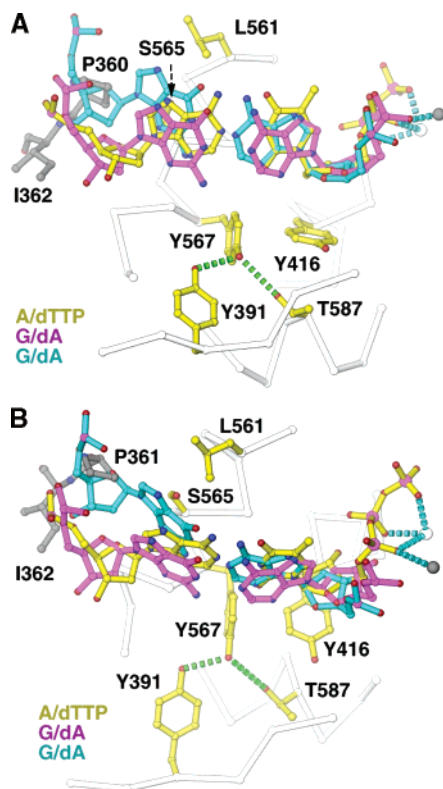
FIGURE 5: Modeling the dA−G mismatch into the ternary RB69 pol complex (*29*). The mismatch was taken from ref *44* (PDB accession number 1NK0) and imported into the ternary RB69 pol structure by superposition of four atoms that define either the two glycosidic bonds (magenta) or the primer glycosidic bond plus its plane (cyan). Panels A and B are two orthogonal views of the model.

FIGURE 6: Modeling the dTTP−C mismatch into the ternary RB69 pol structure (*29*). The dTTP−C mismatch was taken from ref *44* (PDB accession number 1NJZ) and imported into the ternary RB69 pol structure by superposition of four atoms of two glycosidic bonds (cyan) and of all the common dTTP atoms (magenta). The displacement of the templating C (magenta) as modeled could not occur due to stacking interactions with the product DNA duplex. Panels A and B are two orthogonal views of the model.

moiety of the complementary dTTP in the RB69 pol ternary complex (*34*). In this modeling, the templating G also approaches the side chain of L561 (Figure 4). Its close proximity to L561 explains why selectivity against the dG−G mismatch is substantially reduced when the side chain of L561 is changed to a methyl group in the L561A variant. In addition to the dG−G mispair, another purine−purine mismatch, dA−G, was also examined by computer modeling. With the four atoms defining the two glyosidic bonds of the mispair superimposed onto that of the correct dT−A pair in the ternary complex of RB69 pol, the triphosphate tail of the incoming dATP deviated from the optimal position for catalysis, (as shown in magenta in Figure 5). Since we knew that the alignment of dATP and templating G was adversely affected when they were modeled into the active site of the parental enzyme, the decrease in k_{pol} value for this mispair was not unexpected. On the other hand, when the incoming dATP was overlaid onto the dTTP in the ternary complex, using the four atoms defining the sugar and the base of the incoming dNTP only, the templating base G was forced into a position that clashes with the L561 residue (as shown in cyan in Figure 5). This constraint has been relaxed to a certain extent by removing the bulky side chain of L561 as indicated by the higher misincorporation efficiency exhibited by the L561A variant.

The Structural Basis of Selectivity against the Pyrimidine− Pyrimidine Mismatches. With pyrimidine−pyrimidine mis-matches, their C1′−C1′ distances can be much closer than those of the Watson−Crick base pairs (Table 5). In this case,
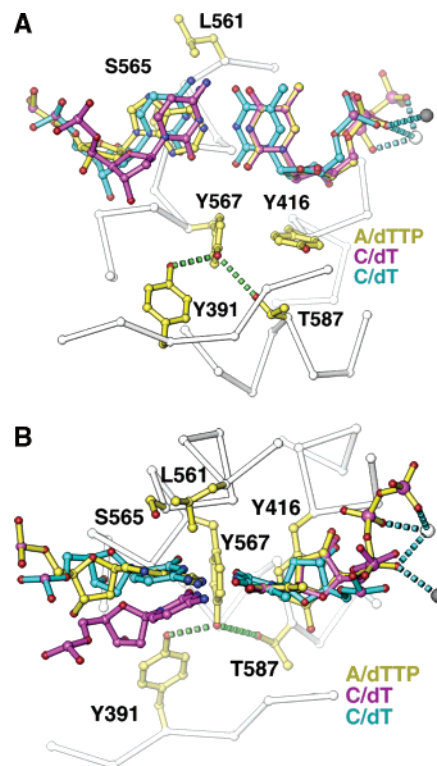
the outcome of modeling depends on the method of superposition between mismatches and the Watson−Crick dT−A base pairs in RB69 pol. When the first method that superimposes four atoms defining two glycosidic bonds of the base pair is used, the dT−C mismatch sits at the midpoint between the side chains of L561 and Y567. When the second method that superimposes four atoms defining the base and glycosidic bond of dTTP is used, the templating nucleotide is displaced substantially due to the noncoplanarity of the mismatch (Figure 6). In the observed C−T (and also A−G) mismatch at the active site of Bst pol I (*44*), the base plane was puckered by about 17°. This base puckering may be specific to a given polymerase with the nascent base pair in the post-insertion site. One would not expect such a puckering geometry in the middle of the DNA duplex or at the nascent base pair of a catalytically competent ternary complex. While ignoring puckering, the sugar and base of the templating nucleotide are displaced much more toward the incoming nucleotides (Figure 6), which substantially reduces contacts between the polymerase and the base. Although these attempts at modeling provide a number of possibilities for how L561 can select against the small size of pyrimidine−pyrimidine mismatches, the precise structural basis for this discrimination is not readily apparent. Solvation of the pyrimidine−pyrimidine mismatches may be involved as previously observed in Bst pol I (*44*) where there is an ordered water molecule between the mismatch and the phenolic side chain corresponding to Y567 of RB69 pol. Thus, selection is mediated by a network of hydrogen bonds

with the solvent. With numerous water molecules near the active site, the dielectric constant will increase in comparison to the situation where there is normal Watson−Crick base pairing; hence, the presence of solvent near the active site would be expected to lower the catalytic efficiency.

Multiple Sources of Selectivity in RB69 DNA Polymerase. Different mismatches have different structural features. DNA polymerases have evolved to exclude them in replication. Some mismatches have shallow minor grooves (for example, dA−C and dC−A) and others have protrusions in the major grooves (for example, dG−G). Discrimination against mismatches may involve many side chains near the nascent base pair and may involve both minor and major grooves.

In summary, the L561A variant generally exhibits an increase in *incorrect* dNTP binding affinity and insertion rate relative to the parental enzyme for mispaired dNTPs. A plausible explanation is that L561 discriminates sterically against mismatches in the nascent base-pair binding pocket by modulating the equilibrium among the open, intermediate, and closed forms of the fingers subdomain. As a consequence, the more perturbing the mismatch, the lower the chances that the nascent base-pair binding pocket will be closed, thus, reducing the probability that the essential, neighboring K560 residue will interact with the triphosphate of the incoming dNTP (*32*). This would be expected to reduce the rate of misinsertion. Alanine substitution for L561 increases the chance for the fingers to close in the presence of a mismatched incoming dNTP so that K560 is more likely to participate in catalysis. Further studies using stopped-flow fluorescence will provide more insight into the way conformational changes influence base selectivity.

ACKNOWLEDGMENT

REFERENCES

1. Kunkel, T. A. (1992) DNA replication fidelity, *J. Biol. Chem. 267*, 18251−4.
2. Echols, H., and Goodman, M. F. (1991) Fidelity mechanisms in DNA replication, *Annu. Rev. Biochem. 60*, 477−511.
3. Goodman, M. F., Creighton, S., Bloom, L. B., and Petruska, J. (1993) Biochemical basis of DNA replication fidelity, *Crit. Rev. Biochem. Mol. Biol. 28*, 83−126.
4. Kunkel, T. A., and Bebenek, K. (2000) DNA replication fidelity, *Annu. Rev. Biochem. 69*, 497−529.
5. Yin, Y. W., and Steitz, T. A. (2002) Structural basis for the transition from initiation to elongation transcription in T7 RNA polymerase, *Science 298*, 1387−95.
6. Goodman, M. F. (2002) Error-prone repair DNA polymerases in prokaryotes and eukaryotes, *Annu. Rev. Biochem. 71*, 17−50.
7. Ellenberger, T., and Silvian, L. F. (2001) The anatomy of infidelity, *Nat. Struct. Biol. 8*, 827−8.
8. Pham, P., Rangarajan, S., Woodgate, R., and Goodman, M. F. (2001) Roles of DNA polymerases V and II in SOS-induced error-prone and error-free repair in *Escherichia coli*, *Proc. Natl. Acad. Sci. U.S.A. 98*, 8350−4.
9. Sutton, M. D., and Walker, G. C. (2001) Managing DNA polymerases: coordinating DNA replication, DNA repair, and DNA recombination, *Proc. Natl. Acad. Sci. U.S.A. 98*, 8342−9.
10. Woodgate, R. (1999) A plethora of lesion-replicating DNA polymerases, *Genes Dev. 13*, 2191−5.
11. Shen, X., Sayer, J. M., Kroth, H., Ponten, I., O'Donnell, M., Woodgate, R., Jerina, D. M., and Goodman, M. F. (2002) Efficiency and accuracy of SOS-induced DNA polymerases replicating benzo[*a*]pyrene-7,8-diol 9,10-epoxide A and G adducts, *J. Biol. Chem. 277*, 5265−74.
12. Freisinger, E., Grollman, A. P., Miller, H., and Kisker, C. (2004) Lesion (in)tolerance reveals insights into DNA replication fidelity, *EMBO J. 23*, 1494−505.
13. Friedberg, E. C., Fischhaber, P. L., and Kisker, C. (2001) Error-prone DNA polymerases: novel structures and the benefits of infidelity, *Cell 107*, 9−12.
14. Hubscher, U., Maga, G., and Spadari, S. (2002) Eukaryotic DNA polymerases, *Annu. Rev. Biochem. 71*, 133−63.
15. Prakash, S., and Prakash, L. (2002) Translesion DNA synthesis in eukaryotes: a one- or two-polymerase affair, *Genes Dev. 16*, 1872−83.
16. Ling, H., Boudsocq, F., Woodgate, R., and Yang, W. (2001) Crystal structure of a Y-family DNA polymerase in action: a mechanism for error-prone and lesion-bypass replication, *Cell 107*, 91−102.
17. Zhou, B. L., Pata, J. D., and Steitz, T. A. (2001) Crystal structure of a DinB lesion bypass DNA polymerase catalytic fragment reveals a classic polymerase catalytic domain, *Mol. Cell 8*, 427−37.
18. Ohmori, H., Friedberg, E. C., Fuchs, R. P., Goodman, M. F., Hanaoka, F., Hinkle, D., Kunkel, T. A., Lawrence, C. W., Livneh, Z., Nohmi, T., Prakash, L., Prakash, S., Todo, T., Walker, G. C., Wang, Z., and Woodgate, R. (2001) The Y-family of DNA polymerases, *Mol. Cell 8*, 7−8.
19. Kunkel, T. A., Pavlov, Y. I., and Bebenek, K. (2003) Functions of human DNA polymerases eta, kappa and iota suggested by their properties, including fidelity with undamaged DNA templates, *DNA Repair 2*, 135−49.
20. Friedberg, E. C., Wagner, R., and Radman, M. (2002) Specialized DNA polymerases, cellular survival, and the genesis of mutations, *Science 296*, 1627−30.
21. Boudsocq, F., Ling, H., Yang, W., and Woodgate, R. (2002) Structure-based interpretation of missense mutations in Y-family DNA polymerases and their implications for polymerase function and lesion bypass, *DNA Repair 1*, 343−58.
22. Beard, W. A., and Wilson, S. H. (2003) Structural insights into the origins of DNA polymerase fidelity, *Structure 11*, 489−96.
23. Kunkel, T. A. (2004) DNA replication fidelity, *J. Biol. Chem. 279*, 16895−8.
24. Beard, W. A., Shock, D. D., and Wilson, S. H. (2004) Influence of DNA structure on DNA polymerase beta active site function: extension of mutagenic DNA intermediates, *J. Biol. Chem. 279*, 31921−9.
25. Braithwaite, D. K., and Ito, J. (1993) Compilation, alignment, and phylogenetic relationships of DNA polymerases, *Nucleic Acids Res. 21*, 787−802.
26. Wang, J., Sattar, A. K., Wang, C. C., Karam, J. D., Konigsberg, W. H., and Steitz, T. A. (1997) Crystal structure of a pol alpha family replication DNA polymerase from bacteriophage RB69, *Cell 89*, 1087−99.
27. Shamoo, Y., and Steitz, T. A. (1999) Building a replisome from interacting pieces: sliding clamp complexed to a peptide from DNA polymerase and a polymerase editing complex, *Cell 99*, 155−66.
28. Hogg, M., Wallace, S. S., and Doublie, S. (2004) Crystallographic snapshots of a replicative DNA polymerase encountering an abasic site, *EMBO J. 23*, 1483−93.
29. Franklin, M. C., Wang, J., and Steitz, T. A. (2001) Structure of the replicating complex of a pol alpha family DNA polymerase, *Cell 105*, 657−67.
30. Joyce, C. M., and Steitz, T. A. (1994) Function and structure relationships in DNA polymerases, *Annu. Rev. Biochem. 63*, 777−822.
31. Yang, G., Franklin, M., Li, J., Lin, T. C., and Konigsberg, W. (2002) A conserved Tyr residue is required for sugar selectivity in a Pol α DNA polymerase, *Biochemistry 41*, 10256−61.
32. Yang, G., Franklin, M., Li, J., Lin, T. C., and Konigsberg, W. (2002) Correlation of the kinetics of finger domain mutants in RB69 DNA polymerase with its structure, *Biochemistry 41*, 2526−34.
33. Bebenek, A., Dressman, H. K., Carver, G. T., Ng, S., Petrov, V., Yang, G., Konigsberg, W. H., Karam, J. D., and Drake, J. W. (2001) Interacting fidelity defects in the replicative DNA polymerase of bacteriophage RB69, *J. Biol. Chem. 276*, 10387−97.

34. Yang, G., Wang, J., and Konigsberg, W. (2005) Base selectivity is impaired by mutants that perturb hydrogen bonding networks in the RB69 DNA polymerase active site, *Biochemistry 44*, 3338–46.

35. Minnick, D. T., Bebenek, K., Osheroff, W. P., Turner, R. M., Jr., Astatke, M., Liu, L., Kunkel, T. A., and Joyce, C. M. (1999) Side chains that influence fidelity at the polymerase active site of *Escherichia coli* DNA polymerase I (Klenow fragment), *J. Biol. Chem. 274*, 3067–75.

36. Minnick, D. T., Liu, L., Grindley, N. D., Kunkel, T. A., and Joyce, C. M. (2002) Discrimination against purine-pyrimidine mispairs in the polymerase active site of DNA polymerase I: a structural explanation, *Proc. Natl. Acad. Sci. U.S.A. 99*, 1194–9.

37. Wang, C. X., Zakharova, E., Li, J., Joyce, C. M., Wang, J., and Konigsberg, W. (2004) Pre-steady-state kinetics of RB69 DNA polymerase and its exo domain mutants: effect of pH and thiophosphoryl linkages on 3′–5′ exonuclease activity, *Biochemistry 43*, 3853–61.

38. Dressman, H. K., Wang, C. C., Karam, J. D., and Drake, J. W. (1997) Retention of replication fidelity by a DNA polymerase functioning in a distantly related environment, *Proc. Natl. Acad. Sci. U.S.A. 94*, 8042–6.

39. Petrov, V. M., and Karam, J. D. (2002) RNA determinants of translational operator recognition by the DNA polymerases of bacteriophages T4 and RB69, *Nucleic Acids Res. 30*, 3341–8.

40. Wang, C. C., Yeh, L. S., and Karam, J. D. (1995) Modular organization of T4 DNA polymerase. Evidence from phylogenetics, *J. Biol. Chem. 270*, 26558–64.

41. Beard, W. A., Shock, D. D., Vande Berg, B. J., and Wilson, S. H. (2002) Efficiency of correct nucleotide insertion governs DNA polymerase fidelity, *J. Biol. Chem. 277*, 47393–8.

42. Kennard, O. (1986) Base-pair mismatches in DNA fragments, *Biochem. Soc. Trans. 14*, 207–10.

43. Bebenek, A., Carver, G. T., Dressman, H. K., Kadyrov, F. A., Haseman, J. K., Petrov, V., Konigsberg, W. H., Karam, J. D., and Drake, J. W. (2002) Dissecting the fidelity of bacteriophage RB69 DNA polymerase: site-specific modulation of fidelity by polymerase accessory proteins, *Genetics 162*, 1003–18.

44. Johnson, S. J., and Beese, L. S. (2004) Structures of mismatch replication errors observed in a DNA polymerase, *Cell 116*, 803–16.

45. Skelly, J. V., Edwards, K. J., Jenkins, T. C., and Neidle, S. (1993) Crystal structure of an oligonucleotide duplex containing G·G base pairs: influence of mispairing on DNA backbone conformation, *Proc. Natl. Acad. Sci. U.S.A. 90*, 804–8.

46. Jang, S. B., Hung, L. W., Chi, Y. I., Holbrook, E. L., Carter, R. J., and Holbrook, S. R. (1998) Structure of an RNA internal loop consisting of tandem C-A$^+$ base pairs, *Biochemistry 37*, 11726–31.

47. Hunter, W. N., Brown, T., Anand, N. N., and Kennard, O. (1986) Structure of an adenine-cytosine base pair in DNA and its implications for mismatch repair, *Nature 320*, 552–5.

48. Brown, T., Hunter, W. N., Kneale, G., and Kennard, O. (1986) Molecular structure of the G.A base pair in DNA and its implications for the mechanism of transversion mutations, *Proc. Natl. Acad. Sci. U.S.A. 83*, 2402–6.

49. Boulard, Y., Cognet, J. A., and Fazakerley, G. V. (1997) Solution structure as a function of pH of two central mismatches, C·T and C·C, in the 29 to 39 K-ras gene sequence, by nuclear magnetic resonance and molecular dynamics, *J. Mol. Biol. 268*, 331–47.